

偏振及光源不敏感的光子晶体平板透镜

岑源, 谢建澜, 刘建军*

(湖南大学 物理与微电子科学学院 微纳光电器件及应用教育部重点实验室、低维结构物理与器件湖南省重点实验室,
湖南 长沙 410082)

摘要: 提出了一种散射子尺寸梯度型光子晶体平板透镜, 该透镜在 TM 偏振和 TE 偏振模式下可同时实现对点光源的成像及对平面波的聚焦, 且在 TM 偏振模式下成像及聚焦均突破了衍射极限, 而在 TE 模式下均实现了亚波长成像及聚焦。该平板透镜无需任何偏振附加组件便可实现偏振不敏感成像及聚焦, 有望用于设计多功能新型光学偏振不敏感成像及聚焦器件, 可应用于实时生物显示、高密度光存储及微电子光刻等领域, 提高梯度光子晶体平板透镜的应用潜力。

关 键 词: 光子晶体; 偏振不敏感; 平板透镜; 点光源成像; 平面波聚焦

中图分类号:O734 文献标识码: A

A photonic crystal flat lens insensitive to polarization mode and light source

CEN Yuan, XIE Jian-lan, LIU Jian-jun*

(Key Laboratory for Micro/Nano Optoelectronic Devices of Ministry of Education & Hunan Provincial Key Laboratory of Low-Dimensional Structural Physics and Devices, School of Physics and Electronics, Hunan University, Changsha 410082, China)

Abstract: A scatterer-size gradient photonic crystal flat lens is proposed, which can simultaneously realize point source imaging and plane wave focusing in TM and TE polarization modes, and both imaging and focusing break through the diffraction limit in TM polarization mode, and realize sub-wavelength imaging and focusing in TE polarization mode. This flat lens can realize polarization-insensitive imaging and focusing without any additional polarization components. It is expected to be used in the design of multi-functional optical polarization-insensitive imaging and focusing devices, and can be applied to real-time biological display, high-density optical storage and microelectronic lithography, and improve the application potential of gradient PC flat lens.

Key words: photonic crystal, polarization mode insensitive, flat lens, point source imaging, plane wave focusing

PACS:42. 25. Bs, 42. 25. Fx, 42. 70. Qs, 42. 79. Bh

引言

光子晶体^[1-3]是一种介电常数按周期或准周期排布且晶格常数为光波长量级的人工微结构材料, 其影响电磁波传播的方式与半导体中的周期性电位类似。因其具有特殊的色散特性、良好的负折射效应及低损耗等优点而在光纤^[4-10]、激光器^[11-12]、滤波器^[13-14]、传感器^[6,9,15-18]、波导^[19-24]及透镜^[25-38]等光

学集成领域得到了广泛应用。

光子晶体在某些频段内存在负折射可用于实现超分辨成像^[39]。超分辨成像可应用于实时生物显示、高密度光存储及微电子光刻等领域, 具有广阔的应用前景^[40]。近年来, 研究人员通过逐步优化散射子尺寸^[31]或折射率^[32]、晶格常数^[33]、梯度晶格间距^[38]等方法来设计梯度光子晶体平板透镜, 并研究了其对平面波的聚焦特性, 给光子晶体平板透镜

收稿日期:2021-05-28,修回日期:2022-01-10

Received date:2021-05-28, Revised date:2022-01-10

基金项目:国家自然科学基金(61405058, 62075059), 湖南省自然科学基金(2017JJ2048, 2020JJ4161)

Foundation items: Supported by National Natural Science Foundation of China (61405058, 62075059), Natural Science Foundation of Hunan Province (2017JJ2048, 2020JJ4161)

作者简介(Biography):岑源(1998-),男,广西百色人,本科生,主要研究领域为光子晶体器件。E-mail: cenyuan2016@163. com

*通讯作者(Corresponding author): E-mail: jianjun.liu@hnu.edu.cn

带来了新的应用前景。

在不同的偏振模式下,光入射光子晶体时会受到不同的影响。散射子折射率梯度^[35]及尺寸梯度^[36]光子晶体平板透镜均可实现对点光源的成像及对平面波的聚焦,但仅限于TM偏振。环形散射子光子晶体平板透镜可实现偏振不敏感成像,但仅限于点光源^[29]。晶格常数梯度型光子晶体平板透镜可实现偏振不敏感聚焦,但仅限于平面波^[33]。由此可知,以往研究的透镜都只适用于特定的偏振模式或特定的入射光源,限制了光子晶体平板透镜的应用范围。为提高光子晶体平板透镜在实时生物显示、高密度光存贮及微电子光刻等领域的应用潜力,无需任何偏振附加组件便可在TM偏振和TE偏振模式下同时实现点光源成像和平面波聚焦的平板透镜亟待研究。本文设计了一种能在TM偏振和TE偏振模式下同时实现点光源成像和平面波聚焦的散射子尺寸梯度光子晶体平板透镜。

1 模型与理论

本文提出的散射子尺寸梯度型光子晶体平板透镜模型,如图1所示。

晶格常数为 $a = 1 \mu\text{m}$,散射子半径在 X 轴方向上保持不变,最中间一行散射子半径 $r_0 = 0.29a$,并沿 $\pm Y$ 方向线性增加,从中间开始往上下两侧的第 i 行散射子的半径 $r_i = r_0 + 0.01 \times i$ 。散射子材料设为锗,其折射率为 $n_{\text{Ge}} = 4$,背景材料设为空气。平板透镜的宽度为 $w = (20\sqrt{3} + 0.998)a$,厚度为 $d = 9.98a$,点光源物距为 $u = d/2$,点光源成像的像距和平面波聚焦的焦距分别为 $v_1 = x_1 - d/2$ 和 $v_2 = x_2 - d/2$ 。

本文采用有限元法对光子晶体的能带及等频面进行计算。在光子晶体中,光的折射方向由群速度决定,群速度与波矢 k 的矢量关系如下^[39]:

$$\mathbf{v}_g = \nabla_k \omega(k) \quad . \quad (1)$$

由此可知,等频面上某一点的群速度垂直于该点等频面的切线且其方向为由频率低的等频面指向频率高的等频面。因此,可利用等频面来分析对应频率的光在光子晶体中的传播方向。

因散射子尺寸呈梯度变化,即该光子晶体并非周期性的,故需通过计算不同散射子半径的普通光子晶体的能带结构及等频面来表征分析散射子尺寸梯度型光子晶体平板透镜的光学特性。首先,计算了等间隔散射子半径的普通光子晶体TM、TE偏

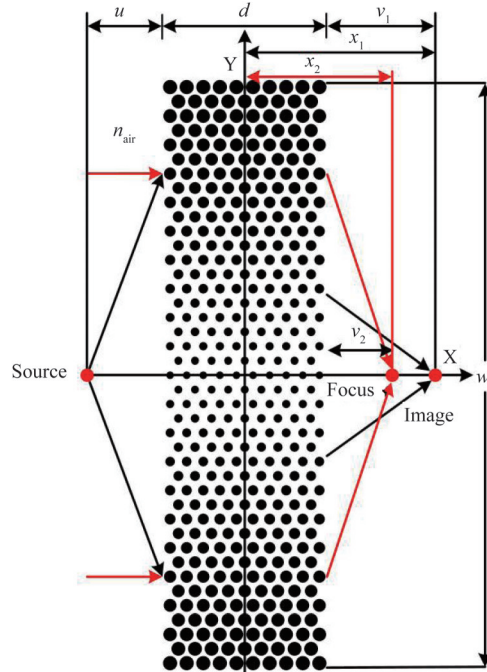


图1 二维三角晶格散射子尺寸梯度型光子晶体平板透镜模型:红色箭头代表平面波聚焦的光路示意图,黑色箭头代表点光源成像的光路示意图

Fig. 1 The model of two-dimensional (2D) triangular lattice PC flat lens with scatterer-size gradient: The red arrow represents the light path of plane wave focusing, and the black arrow represents the light path of point source imaging

振的能带结构及等频面,如图2(a-h)所示。其次,利用等频面法分析TM、TE偏振模式下光在光子晶体中的传播方向,如图2(i)和2(j)所示。

普通光子晶体平板透镜利用负有效折射率可使点光源成像^[26]。入射光波长取 $\lambda = 3.303 \mu\text{m}$ 为例,即 $f = a/\lambda = 0.303$ 。由图2(a)可知,入射光频率处于第二能带频段内。由图2(c-e)和2(i)可知,等频面频率由中心沿径向向外逐渐降低且入射光束和折射光束位于法线的同侧,故散射子尺寸梯度型光子晶体平板透镜具有负折射效应。因此,散射子尺寸梯度型光子晶体平板透镜在TM偏振模式下可实现对点光源的成像。由图2(b)可知,当散射子半径不同时,入射光频率所处的能带频段也不同。通过大量仿真计算可知,当普通光子晶体散射子半径在 $r \in [0.30 \mu\text{m}, 0.38 \mu\text{m}]$ 范围内时,入射光的频率处于带隙频段内。因此,分别计算了 $r = 0.39 \mu\text{m}$, $0.44 \mu\text{m}$ 及 $0.49 \mu\text{m}$ 的TE偏振等频面,如图2(f-h)所示。由图2(f-h)和2(j)可知,当散射子半径不断增大时,从 $r = 0.44 \mu\text{m}$ 开始具有负折射效应,通过验

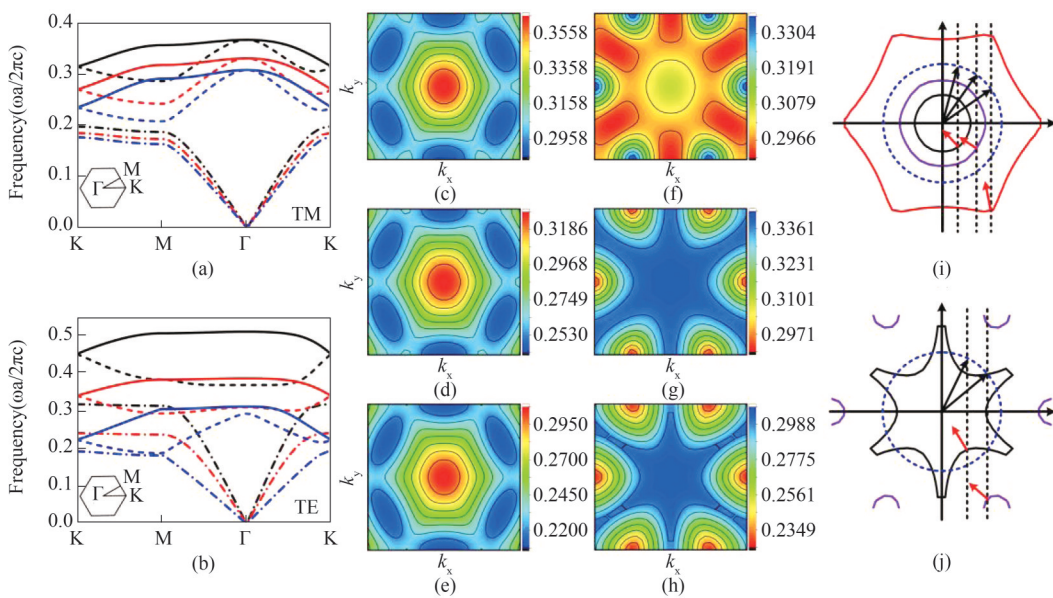


图2 (a) $r = 0.29 \mu\text{m}$ (黑), $0.34 \mu\text{m}$ (红), $0.39 \mu\text{m}$ (蓝)的普通光子晶体的TM偏振能带结构;(b) $r = 0.29 \mu\text{m}$ (黑), $0.39 \mu\text{m}$ (红), $0.49 \mu\text{m}$ (蓝)的普通光子晶体的TE偏振能带结构。点划线、虚线、实线分别表示第一、第二及第三能带。普通光子晶体的第二能带TM偏振等频面:(c) $r = 0.29 \mu\text{m}$; (d) $r = 0.34 \mu\text{m}$; (e) $r = 0.39 \mu\text{m}$ 。普通光子晶体的TE偏振等频面:(f) $r = 0.39 \mu\text{m}$ (第二能带);(g) $r = 0.44 \mu\text{m}$ (第三能带);(h) $r = 0.49 \mu\text{m}$ (第三能带);(i)红色、紫色和黑色实线分别代表(c-e)对应于入射光频率的等频线;(j)紫色和黑色实线分别代表(g-h)对应于入射光频率的等频线,因(f)无负折射而不再对其单独研究;蓝色虚线为光锥等频线。黑色箭头是入射光束,从空中入射到光子晶体中。红色箭头是光束在光子晶体中的传播方向,即折射光束。(i)和(j)仅是一个示意图^[35-36]。

Fig. 2 (a) TM polarization band structure of common photonic crystal (CPC) with $r = 0.29 \mu\text{m}$ (black), $0.34 \mu\text{m}$ (red) and $0.39 \mu\text{m}$ (blue). (b) TE polarization band structure of CPC with $r = 0.29 \mu\text{m}$ (black), $0.39 \mu\text{m}$ (red) and $0.49 \mu\text{m}$ (blue). Dot dash line, dot line and solid line represent the first, second and third bands respectively. The EFL of the second TM polarization band of CPC: (c) $r = 0.29 \mu\text{m}$, (d) $r = 0.34 \mu\text{m}$, (e) $r = 0.39 \mu\text{m}$. The EFL of TE polarization band of CPC: (f) $r = 0.39 \mu\text{m}$ (the second band), (g) $r = 0.44 \mu\text{m}$ (the third band), (h) $r = 0.49 \mu\text{m}$ (the third band). (i) The red, purple and black solid lines represent (c), (d) and (e) EFL corresponding to the incident light source frequency, respectively. (j) The purple and black solid lines represent (g) and (h) EFL corresponding to the incident light source frequency, respectively. Because (f) has no negative refraction, it is no longer studied separately. The blue dot line is EFL of light cone. The black arrow is an incident beam, incident from the air into the PC. The red arrow is the propagation direction of the beam in the PC, that is, the refracted beam. (i) and (j) are only schematic diagrams^[35-36].

证其它半径($r \in [0.44 \mu\text{m}, 0.49 \mu\text{m}]$)散射子的等频面也可实现负折射。因此,散射子尺寸梯度型光子晶体平板透镜在TE偏振模式下可实现对点光源的成像。

由于空气是各向同性均匀介质(圆形色散曲线),故在入射透镜前平面波通常是衍射的。在平面波进入透镜后,由于凸形归一化频率曲线,会产生负衍射^[41-42],光被迫将其波前转换为所需的凸形,故能实现对平面波的聚焦。由图2(c-e)可知,TM偏振等频面的归一化频率曲线为凸型。因此,散射子尺寸梯度型光子晶体平板透镜在TM偏振模式下可实现对平面波的聚焦。由图2(g-h)可知,从 $r =$

$0.44 \mu\text{m}$ 开始TE偏振等频面的归一化频率曲线为凸型,通过验证其它半径($r \in [0.44 \mu\text{m}, 0.49 \mu\text{m}]$)散射子的TE偏振等频面的归一化频率曲线也为凸型。因此,散射子尺寸梯度型光子晶体平板透镜在TE偏振模式下可实现对平面波的聚焦。

2 结果与讨论

由上述的分析可知,散射子尺寸梯度型光子晶体平板透镜在TM偏振和TE偏振模式下可同时实现对点光源的成像及对平面波的聚焦,其实现偏振不敏感成像及聚焦的范围为 $f \in [90.5 \text{ THz}, 91.0 \text{ THz}]$ (仅为一部分范围)。取 $\lambda = 3.303 \mu\text{m}$ (90.84 THz)为例,TM偏振和TE偏振模式下相应的成像及聚焦特性如图3所示。

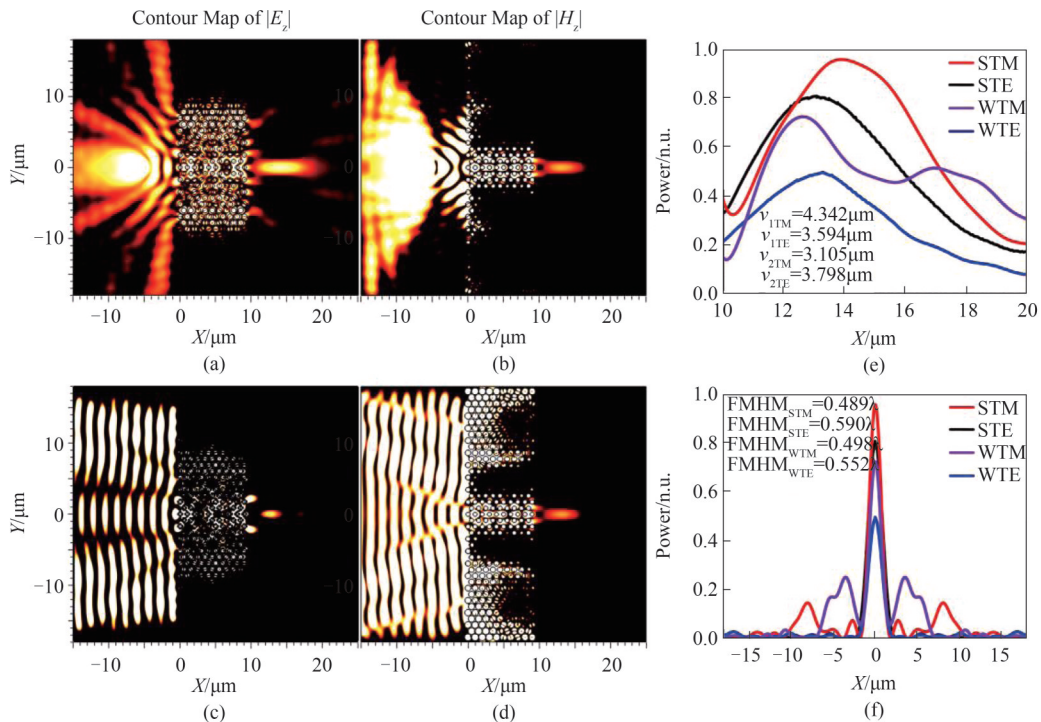


图3 取 $\lambda = 3.303 \mu\text{m}$ (90.84 THz)为例。点光源激发的球面波入射散射子尺寸梯度型光子晶体平板透镜的场分布:(a)TM偏振模式;(b)TE偏振模式。平面波入射散射子尺寸梯度型光子晶体平板透镜的场分布:(c)TM偏振模式;(d)TE偏振模式。在TM、TE偏振模式下,点光源(PS)成像及平面波(PW)聚焦的场功率:(e)轴平面;(f)像平面及焦平面。STM和STE分别代表在TM、TE偏振模式下点光源成像的场功率;WTM和WTE分别代表在TM、TE偏振模式下平面波聚焦的场功率。

Fig. 3 Take $\lambda = 3.303 \mu\text{m}$ (90.84 THz) as an example. The field distribution of spherical wave stimulated by point source incident on the PC flat lens with scatterer-size gradient: (a) TM polarization mode. (b) TE polarization mode. The field distribution of plane wave incident on the PC flat lens with scatterer-size gradient: (c) TM polarization mode. (d) TE polarization mode. In TM and TE polarization modes, the field power of point source (PS) imaging and plane wave (PW) focusing: (e) axis plane (f) image plane and focal plane. STM and STE represent the field power of point source imaging in TM and TE polarization modes respectively. WTM and WTE represent the field power of plane wave focusing in TM and TE polarization modes respectively.

由图3(a-d)可知,散射子尺寸梯度型光子晶体平板透镜在TM、TE偏振模式下可同时实现对点光源的成像及对平面波的聚焦。由图3(e)可知,其像距及焦距分别为 $v_{1\text{TM}} = 4.342 \mu\text{m}$ 、 $v_{2\text{TM}} = 3.105 \mu\text{m}$, $v_{1\text{TE}} = 3.594 \mu\text{m}$ 、 $v_{2\text{TE}} = 3.798 \mu\text{m}$,且均小于 $d/2$,点光源成像的物距与像距之和均小于透镜厚度。由图3(f)可知,半高宽为 $\text{FWHM}_{\text{STM}} = 0.489\lambda$, $\text{FWHM}_{\text{WTM}} = 0.498\lambda$, $\text{FWHM}_{\text{STE}} = 0.590\lambda$, $\text{FWHM}_{\text{WTE}} = 0.552\lambda$,即透镜对点光源的成像及对平面波的聚焦,在TM偏振模式下均突破了衍射极限,而在TE模式下均实现了亚波长成像及聚焦。

3 结论

本文提出的散射子尺寸梯度型光子晶体平板透镜在TM、TE偏振模式下同时实现了对点光源的成像及对平面波的聚焦,在TM偏振模式下均突破

了衍射极限,而在TE模式下均实现了亚波长成像及聚焦。

References

- [1] Yablonovitch E. Inhibited spontaneous emission in solid-state physics and electronics [J]. *Phys. Rev. Lett.*, 1987, **58**(20): 2059–62.
- [2] John S. Strong localization of photons in certain disordered dielectric super-lattices [J]. *Phys. Rev. Lett.*, 1987, **58**(23): 2486–9.
- [3] Chan Y, Chan C, Liu Z. Photonic band gaps in two dimensional photonic quasicrystals [J]. *Phys. Rev. Lett.*, 1998, **80**(5): 956–9.
- [4] Markos C, Travers J, Abdolvand A, et al. Hybrid photonic-crystal fiber [J]. *Rev. Mod. Phys.*, 2017, **89**(4): 045003.
- [5] Han J, Liu E, Liu J. Circular gradient-diameter photonic crystal fiber with large mode area and low bending loss [J]. *J. Opt. Soc. Am. A*, 2019, **36**(4): 533–9.
- [6] Liu Q, Yan B, Liu J. U-shaped photonic quasi-crystal fiber sensor with high sensitivity based on surface plasmon

- resonance [J]. *Appl. Phys. Express*, 2019, **12**(5): 052014.
- [7] Liu E, Liang S, Liu J. Double-cladding structure dependence of guiding characteristics in six-fold symmetric photonic quasi-crystal fiber [J]. *Superlattices Microstruct.*, 2019, **130**: 61–6.
- [8] Liu E, Tan W, Yan B, et al. Robust transmission of orbital angular momentum mode based on a dual-cladding photonic quasi-crystal fiber [J]. *J. Phys. D: Appl. Phys.*, 2019, **52**(32): 325110.
- [9] Li C, Yan B, Liu J. Refractive index sensing characteristics in a D-shaped photonic quasi-crystal fiber sensor based on surface plasmon resonance [J]. *J. Opt. Soc. Am. A*, 2019, **36**(10): 1663–8.
- [10] Huo Z, Liu E, Liu J. Hollow-core photonic quasicrystal fiber with high birefringence and ultra-low nonlinearity [J]. *Chin. Opt. Lett.*, 2020, **18**(3): 030603.
- [11] Bakoz A, Liles A, Gonzalez-Fernandez A, et al. Wavelength stability in a hybrid photonic crystal laser through controlled nonlinear absorptive heating in the reflector [J]. *Light Sci. & Appl.*, 2018, **7**(1): 39.
- [12] Shao H, Ying G, He H, et al. Purcell enhancement of a deterministically coupled quantum dot in an SU-8 laser patterned photonic crystal heterostructure [J]. *Appl. Phys. Lett.*, 2020, **117**(4): 043103.
- [13] Zhao Y, Wang Z, Jiang Z, et al. Add-drop filter with compound structures of photonic crystal and photonic quasicrystal [J]. *J. Infrared Millim. Waves*, 2017, **36**(3): 342–8.
- [14] Liu L, Liao S. Low-power active tunable microwave photonic filter using photonic crystal nanocavities [J]. *IEEE Photonic Tech. L.*, 2020, **32**(16): 999–1002.
- [15] Ge R, Yan B, Xie J, et al. Refractive index sensor with high sensitivity based on circular photonic crystal [J]. *J. Opt. Soc. Am. A*, 2018, **35**(6): 992–7.
- [16] Shi A, Ge R, Liu J. Refractive index sensor based on photonic quasi-crystal with concentric ring microcavity [J]. *Superlattices Microstruct.*, 2019, **133**: 106198.
- [17] Shi A, Ge R, Liu J. Side-coupled liquid sensor and its array with magneto-optical photonic crystal [J]. *J. Opt. Soc. Am. A*, 2020, **37**(8): 1244–8.
- [18] Ge R, Yan B, Xie J, et al. Logic gates based on edge states in gyromagnetic photonic crystal [J]. *J. Magn. Magn. Mater.*, 2020, **500**(15): 166367.
- [19] Wang Z, Su K, Feng B, et al. Coupling length variation and multiwavelength demultiplexing in photonic crystal waveguides [J]. *Chin. Opt. Lett.*, 2018, **16**(011): 011301.
- [20] Yan B, Xie J, Liu E, et al. Topological edge state in the two-dimensional stampfli-triangle photonic crystals [J]. *Phys. Rev. Applied*, 2019, **12**(4): 044004.
- [21] Hou T, Ge R, Tan W, et al. One-way rotating state of multi-periodicity frequency bands in circular photonic crystal [J]. *J. Phys. D: Appl. Phys.*, 2020, **53**(7): 075104.
- [22] Guo Z, Yan B, Liu J. Straight lined and circular interface states insunflower-type photonic crystals [J]. *J. Opt.*, 2020, **22**(3): 035002.
- [23] Peng Y, Yan B, Xie J, et al. Variation of topological edge states of 2D honeycomb lattice photonic crystals [J]. *Phys. Status Solidi – R*, 2020, **14**(9): 2000202.
- [24] Shi A, Yan B, Ge R, et al. Coupled cavity-waveguide based on topological corner state and edge state [J]. *Opt. Lett.*, 2021, **46**(5): 1089–1092.
- [25] Li Z, Lin L. Evaluation of lensing in photonic crystal slabs exhibiting negative refraction [J]. *Phys. Rev. B*, 2003, **68**(24): 245110.
- [26] Berrier A, Mulot M, Swillo M, et al. Negative refraction at infrared wavelengths in a two-dimensional photonic crystal [J]. *Phys. Rev. Lett.*, 2004, **93**(7): 073902.
- [27] Feng Z, Zhang X, Wang Y, et al. Negative refraction and imaging using 12-fold-symmetry quasicrystals [J]. *Phys. Rev. Lett.*, 2005, **94**(24): p.247402.1–247402.4.
- [28] Fang Y. Imaging by photonic crystal without negative refraction [J]. *Laser Phys. Lett.*, 2010, **2**(10): 502–5.
- [29] Wu H, Jiang L, Jia W, et al. Imaging properties of an annular photonic crystal slab for both TM-polarization and TE-polarization [J]. *J. Opt.*, 2011, **13**(9): 095103.
- [30] Fang Y, Yang L, Zhou J. Tamm states of one-dimensional photonic crystal based on surface defect [J]. *J. Infrared Millim. Waves*, 2013, **32**(6): 526–30.
- [31] Gaufillet F, Akmanoy E. Design and experimental evidence of a flat graded-index photonic crystal lens [J]. *J. Appl. Phys.*, 2013, **114**(8): 12–3.
- [32] Gaufillet F, Akmanoy E. Design of flat graded index lenses using dielectric graded photonic crystals [J]. *Opt. Mater.*, 2015, **47**(9): 555–60.
- [33] Turduev M, Bor E, Kurt H. Photonic crystal based polarization insensitive flat lens [J]. *J. Phys. D: Appl. Phys.*, 2017, **50**(27): 275105.
- [34] Qi Y, Sun X, Wang S, et al. Design of an electrically tunable micro-lens based on graded photonic crystal [J]. *Crystals*, 2018, **8**: 303.
- [35] Xie J, Wang J, Ge R, et al. Multiband super-resolution imaging of graded-index photonic crystal flat lens [J]. *J. Phys. D: Appl. Phys.*, 2018, **51**(20): 205103.
- [36] Cen Y, Xie J, Liu J. Multi-band imaging and focusing of photonic crystal flat lens with scatterer-size-gradient [J]. *Chin. Opt. Lett.*, 2019, **17**(8): 080501.
- [37] Zhao H, Xie J, Liu J. An approximate theoretical explanation for super-resolution imaging of two-dimensional photonic quasi-crystal flat lens [J]. *Appl. Phys. Express*, 2020, **13**(2): 022007.
- [38] Sheng J, Xie J, Liu J. Multiple super-resolution imaging in the second band of gradient lattice spacing photonic crystal flat lens [J]. *Chin. Opt. Lett.*, 2020, **18**(12): 120501.
- [39] Notomi M. Theory of light propagation in strongly modulated photonic crystals: Refraction like behavior in the vicinity of the photonic band gap [J]. *Phys. Rev. B*, 2000, **62**(16): 10696–705.
- [40] Zhang X, Liu Z. Superlenses to overcome the diffraction limit [J]. *Nat. Mater.*, 2008, **7**(6): 435–41.
- [41] Maigyte L, Purlys V, Trull J, et al. Flat lensing in the visible frequency range by woodpile photonic crystals [J]. *Opt. Lett.*, 2013, **38**(14): 2376–8.
- [42] Kumar N, Herrero R, Botey M, et al. Flat lensing by periodic loss-modulated materials [J]. *J. Opt. Soc. Am. B*, 2013, **30**(10): 2684–8.